# ESCRT-III acts in scissioning new peroxisomes from the ER

Authors: Fred D. Mast[1,2], Thurston Herricks[1,2], Kathleen M. Strehler[1,2], Leslie R. Miller[1,2], Ramsey A. Saleem[1,2,†], Richard R. Rachubinski[3], and John D. Aitchison[1,2,3,*].

1. Center for Infectious Disease Research, 307 Westlake Avenue North, Suite 500, Seattle, Washington, 98109-5219, United States of America
2. Institute for Systems Biology, 401 Terry Avenue North, Seattle, Washington, 98109-5219, United States of America
3. Department of Cell Biology, University of Alberta, 5-14 Medical Sciences Building, Edmonton, Alberta, T6G 2H7, Canada

† Current address: Amgen, 360 Binney Street, Cambridge, Massachusetts, 02142-1011

Corresponding author:
John D. Aitchison, PhD
Center for Infectious Disease Research
307 Westlake Avenue North, Suite 500
Seattle, Washington, 98109-5219
Tel: (206) 256-7470
Fax: (206) 256-7229
john.aitchison@cidresearch.org

Character count without spaces: 14,635

Keywords: peroxisome biogenesis; ESCRT-III; peroxisomes; preperoxisomal vesicles; endoplasmic reticulum; peroxin; Snf7; Vps20; Pex3; Pex19

**Abstract**

Dynamic control of proliferation is integral to the peroxisome's many functions. A breakdown in the ability of cells to form peroxisomes is linked to many human health issues, including defense against infectious agents, cancer, aging, heart disease, obesity and diabetes, and forms the basis of a spectrum of genetic disorders that cause severe neuropathologies. The endoplasmic reticulum (ER) serves as a source for preperoxisomal vesicles (PPVs) that mature into peroxisomes during *de novo* peroxisome biogenesis and to support growth and division of existing peroxisomes. However, the mechanism of PPV formation and release from the ER remains poorly understood. Here we show that the evolutionarily ancient endosomal sorting complexes required for transport (ESCRT)-III are peroxisome biogenesis factors that function to cleave PPVs budding from the ER into the cytosol. Using comprehensive morphological and genetic assays of peroxisome formation and function we find that absence of ESCRT-III proteins impedes *de novo* peroxisome formation and results in an aberrant peroxisome population *in vivo*. Using a cell-free PPV budding assay we show that ESCRT-III proteins Vps20 and Snf7 are required to release PPVs from the ER. ESCRT-III is therefore a positive effector of membrane scission for vesicles budding both away from and towards the cytosol, a finding that has clear implications for the evolutionary timing of emergence of peroxisomes and the rest of the internal membrane architecture of the eukaryotic cell.

## Introduction

Peroxisome proliferation occurs via two partially redundant mechanisms: the division of existing peroxisomes through fission and *de novo* formation from the ER (Mast et al., 2015; Smith and Aitchison, 2013). Fission of peroxisomes is comparatively well characterized, and requires the Pex11 family of proteins to elongate and constrict the organelle, permitting GTP-dependent scission by dynamin related proteins (DRPs) (Schrader et al., 2016). The mechanism of *de novo* formation remains poorly understood and the identities of many factors involved in this process are still unknown (Agrawal and Subramani, 2016).

In yeast, most peroxisomal membrane proteins (PMPs) transit through the ER on their way to peroxisomes (Hoepfner et al., 2005; Schuldiner et al., 2008; Thoms et al., 2012; van der Zand et al., 2010). A global analysis of localized protein synthesis also found that many of these PMPs are likely cotranslated at the ER (Jan et al., 2014).

A vesicular transport pathway exists to transfer proteins and membranes from the ER to peroxisomes (Agrawal et al., 2016; Agrawal et al., 2011; Lam et al., 2010), which is essential even when peroxisomes multiply by growth and division (Mast et al., 2016). Pex3 accumulates initially at an ER subdomain before being released into a PPV that buds from the ER (Halbach et al., 2006; Hoepfner et al., 2005; Tam et al., 2005). Sorting of PMPs through the ER to sites of PPV formation and egress requires both Pex3-dependent and –independent processes (Fakieh et al., 2013). The ER-shaping reticulon proteins,through physical interactions with Pex29 and Pex30, assist in regulating the sorting of Pex3 through the ER and in the release of PPVs (David et al., 2013; Mast et al., 2016). Pex30 and its paralog, Pex31, have membrane shaping

capabilities like the reticulon proteins, which may help in defining and segregating the PPV exit site in the ER from its other functions (Joshi et al., 2016).

The formation of these preperoxisomal vesicles (PPVs) requires Pex3 and Pex19 and their loss leads to an inability of cells to form peroxisomes and consequently, the eventual loss of the organelle (Hettema et al., 2000; Hoepfner et al., 2005). Pex19, a cytosolic protein that interacts with Pex3 and other PMPs, functions as a chaperone and is essential for budding PPVs from the ER. At least two classes of PPVs (V1 and V2) have been characterized (Agrawal et al., 2016; Titorenko et al., 2000; Titorenko and Rachubinski, 2000; van der Zand et al., 2012); both contain Pex3, but differ in the presence or absence of docking-factor or RING finger group proteins of the peroxisomal matrix protein import complex (peroxisomal importomer) (Agrawal et al., 2016). The separation of these two subcomplexes of the importomer could prevent premature assembly in the ER and the import of peroxisomal proteins directly into the ER (Agrawal et al., 2016; van der Zand et al., 2012).While Pex3 and Pex19 are necessary for PPV budding, they are not sufficient, and evidence suggests additional cytosolic component(s) are required, at least one of which likely consumes ATP (Agrawal et al., 2011; Lam et al., 2010). Dynamin-related proteins, which function in peroxisome division, or COPI and COPII vesicle transport pathways, all of which consume GTP, have consistently been shown to not be essential for PPV formation (Lam et al., 2010; Motley et al., 2015; Motley and Hettema, 2007; Perry et al., 2009; South et al., 2000).

Here, we identify a novel role for endosomal sorting complexes required for transport (ESCRT)-III in the *de novo* biogenesis of peroxisomes. In particular, through use of a series of comprehensive morphological and genetic assays of peroxisome formation and function and *in*

*vitro* biochemical assays that produce preperoxisomal vesicles from the ER, we implicate ESCRT-III proteins Vps20 and Snf7 as being essential for the scission of PPVs from the ER.

**Results and discussion**

Screens of an isogenic, arrayed collection of yeast gene deletion strains identified 211 genes whose disruption led to defects in the cells' ability to form peroxisomes (Saleem et al., 2008; Saleem et al., 2010; Smith et al., 2006). We reasoned that these datasets held clues to candidates involved in the *de novo* biogenesis of peroxisomes, and in the formation of PPVs at the ER. *A priori,* candidates would be cytosolic and/or localized to the ER, and would use ATP in their activity. Candidates with these characteristics were components of ESCRT, with a statistically significant hypergeometric p-value of 0.003 (Saleem et al., 2010).

ESCRT is composed of five subcomplexes, including ESCRT-0, -I, -II, -III (and -III-associated) and the AAA-ATPase Vps4 complex (Babst et al., 2002a; Babst et al., 2002b; Babst et al., 1997; Katzmann et al., 2001; Katzmann et al., 2003) (reviewed in (Henne et al., 2011; Schoneberg et al., 2016)). These five complexes function sequentially to mediate the formation of intraluminal vesicles, and also assist in piecemeal fashion with numerous other cellular activities like cytokinesis (Carlton and Martin-Serrano, 2007), plasma membrane repair (Jimenez et al., 2014; Scheffer et al., 2014), autophagosome closure (Lee et al., 2007; Rusten et al., 2007), viral replication and budding (Garrus et al., 2001), nuclear envelope reformation (Olmos et al., 2015; Vietri et al., 2015), nuclear pore complex quality surveillance (Webster et al., 2014), neuronal pruning (Loncle et al., 2015), and microtubule severing(Guizetti et al., 2011) (Henne et al., 2011; Schoneberg et al., 2016). ESCRT-III, composed of Vps20, Snf7, Vps24 and Did4 in yeast, is evolutionarily ancient, and is the primary effector complex for all these

activities (Henne et al., 2011; Tang et al., 2015). Given this wealth of function, particularly for ESCRT-III, a key consideration was whether ESCRTs have a direct role in peroxisome biogenesis or exert indirect effects due to their diversity of activity.

We used our one-cell doubling evaluation of living arrays of yeast (ODELAY!) platform (Herricks et al., 2017) to address the role of ESCRT in peroxisome biogenesis by comparing growth on solid-phase medium containing either glucose or oleic acid, which requires functional peroxisomes for its metabolism, as the sole carbon source (Fig. 1 and Fig. S1). Unlike traditional spot-based assays and assays utilizing optical density measurements at a population level, ODELAY! provides time-resolved measurements of yeast populations from individual strains. ODELAY! therefore permits standardized analyses of the growth rates and population heterogeneity both within and between strains for up to 96 strains measured in parallel across different growth conditions. Strains with general growth defects have comparable normalized growth rates under both conditions, whereas condition-specific strains grow more slowly in one condition versus the other.

Following ODELAY! measurements, population doubling times were normalized, and the mean z-score for each deletion strain was compared between the two growth conditions (Fig. 1). The *pex19*Δ and *pot1*Δ strains, which lack the ability to form peroxisomes (Hettema et al., 2000) or perform the last step of β-oxidation (Igual et al., 1991), respectively, reveal condition-specific growth defects, as they exhibited slightly faster growth in the presence of glucose but grew 4-5 standard deviations slower than *wild-type* in the presence of oleic acid (Fig. 1).

ESCRT-III deletion strains have pronounced condition-specific growth defects in the presence of oleic acid, with *vps20*Δ cells incapable of cell division in oleic acid, while *did4*Δ and

*snf7*Δ cells registered the slowest doubling rates of all ESCRT deletions (Fig. 1). ESCRT-I deletion strains displayed general growth defects whereas ESCRT-II deletion strains tightly clustered, in line with their known structural and functional assembly as a single protein complex, and showed a condition-specific growth defect, although not as severe as ESCRT-III (Fig. 1). Other ESCRT deletion strains also had slower, but less severe than ESCRT-III, doubling times in oleic acid, except for the strain lacking the Vps4 regulator Vta1 which, like the peroxisome inheritance mutants *inp1*Δ and *inp2*Δ, had a faster doubling time than *wild-type* under both conditions (Fig. 1).

To determine if the growth defects observed for ESCRT-III result from defects in peroxisomes we used electron microscopy to investigate the cellular ultrastructure of cells lacking individual components of the core ESCRT-III complex under conditions that promote peroxisome biogenesis conditions (Fig. 2 and Fig. S2). Peroxisomes were readily observed in *wild-type* cells as orbicular structures delimited by a single lipid bilayer and containing an electron-dense, paracrystalline matrix (Fig. 2 A). In contrast, peroxisomes were not observed in *vps20Δ* cells, which instead contained infrequent small vesicular structures attached to ER membranes (Fig. 2 B). In *snf7Δ* cells, peroxisome-like structures lacking a dense matrix were infrequently seen in close apposition to, and possibly contiguous with, the ER (Fig. 2 C). Quantification revealed fewer peroxisomes and peroxisome-like structures for all deletion strains of the ESCRT-III complex (Fig. 2 D and Table 1), although peroxisomes similar in size to *wild-type* peroxisomes were observed in *did4*Δ and *vps24*Δ cells, but at numbers 25% and 45% less, respectively, than peroxisomes in *wild-type* cells (Fig. 2 E – I).

The observed growth and peroxisome morphology defects detected for deletion strains of ESCRT-III and in particular for *vps20*Δ and *snf7*Δ, suggested a role for ESCRT-III in peroxisome biogenesis. To test this, we used an *in vivo* peroxisome biogenesis assay in which tetracycline-control of *PEX19* expression synchronizes cells for *de novo* peroxisome biogenesis without overexpressing peroxins (Fig. 3 A) (Mast et al., 2016). With *PEX19* expressed, 97% of *wild-type* cells contained an average of 10 peroxisomes per cell, as assessed by the punctate localization of peroxisomal Gpd1-GFP. Repression of *PEX19* expression by treatment with doxycycline removed peroxisomes from the yeast population, with only ~1.5% of cells containing on average one peroxisome per cell. Removal of doxycycline led to *de novo* biogenesis of peroxisomes with ~70% of cells containing ~4 peroxisomes per cell after 12 hrs. In contrast, *vps20*Δ and *snf7*Δ had fewer peroxisomes per cell in control conditions and retained more of them, 6% and 11% respectively, following doxycycline treatment. Upon stimulating *de novo* peroxisome biogenesis, *vps20*Δ and *snf7*Δ failed to produce peroxisomes at rates comparable to *wild-type*, revealing a defect in the ability of *vps20*Δ and *snf7*Δ cells to form new peroxisomes *de novo* (Fig. 3 A).

Notably, Snf7 localized to sites of *de novo* peroxisome biogenesis in a tetracycline-regulated *PEX19* background strain. Pex3-GFP and Snf7-mCherry puncta rarely overlap under control conditions, but following doxycycline-treatment to induce *de novo* peroxisome formation, 13.5% of Pex3p-GFP puncta correspondingly colocalized with Snf7-mCherry signal (Fig. 3 Bb). We were unable to detect a meaningful fluorescent signal for Vps20-mCherry under these conditions.

Current models of ESCRT-III function propose that Vps20 is recruited to a membrane first, initiating activation and polymerization of additional members, especially Snf7, to form spirals and coils that deform membranes into tubes or cones to achieve membrane scission (Henne et al., 2011; Schoneberg et al., 2016). Vps24 caps the polymers and stops polymerization, whereas Did4 is integrated into the polymer to promote its disassembly by recruiting the AAA-ATPase, Vps4 (Henne et al., 2011; Schoneberg et al., 2016).

To test if ESCRT-III is required for PPV scission at the ER we used an *in vitro* budding assay that reconstitutes the packaging and release of PMPs from the ER via PPVs (Mast et al., 2016) (Fig. 4). ER membranes were prepared from a *pex19*Δ strain in which Pex3 and other PMPs are trapped in the ER (Agrawal et al., 2016; Agrawal et al., 2011). The release of Pex3 was stimulated by addition of wild-type cytosol and an ATP regeneration system (Lam et al., 2010) but not by cytosol from *pex19*Δ, *vps20*Δ, or *snf7*Δ cells (Fig. 4 A). We also tested cytosols from other ESCRT and ESCRT-III deletion strains, *e.g.*, *did4*Δ, and found that their cytosols still promoted the formation of Pex3-containing PPVs but sometimes at levels less than that produced by *wild-type* cytosol (Fig. 4 A and Fig. S3). Mixing the S100 fraction of cytosols from *snf7*Δ with *vps20Δ* or *pex19Δ* partially complemented the defect in Pex3-GFP release (Fig 4 A). It is known that ESCRT-III does not depend on ATP-hydrolysis to mediate membrane scission but rather relies on the AAA-ATPase Vps4 to remove and recycle ESCRT-III components. Accordingly, treatment of the reaction with apyrase to deplete ATP led to a reduction, but not abrogation, of PPV budding that could be restored to typical levels by addition of exogenous ATP. Consistent with this observation, PPV release occurs rapidly upon reaction mixing,

followed by further incremental release over time, suggesting that ATP acts primarily in recycling scission components (Fig. 4 B).

As classically defined, ESCRT-III, and particularly Vps20 and Snf7, are "peroxins" as they are required for peroxisomal membrane biogenesis and peroxisome proliferation (Distel et al., 1996). Our observations are consistent with a model wherein Vps20 is recruited to sites of PPV formation and, in turn, recruits and activates the polymerization of Snf7 to drive membrane scission and release of the PPV into the cytosol. The other ESCRT-III proteins, Vps24 and Did4, are likely also involved but not essential for PPV scission and probably influence the dynamics of PPV formation and recruit the machinery for disassembly of ESCRT-III at the ER. Consistent with this hypothesis, *did4*Δ displayed severe growth defects when grown in the presence of oleic acid and showed reduced budding of Pex3-positive PPVs from the ER (Fig. 1 and Fig. S3). This is consistent with its role in recruiting the AAA-ATPase Vps4 complex to disassemble ESCRT-III polymers and previous observations that the amount of cytosolic Snf7 is reduced in *did4*Δ cells because it is trapped in a polymerized state on membranes.

ESCRT-III is typically thought to be involved in vesicle budding *away from* the cytosol (reverse-topology membrane scission) with or without other ESCRT complexes (subsets of ESCRT-0, -I and -II) (Henne et al., 2011; Schoneberg et al., 2016). Our data extend ESCRT-III function to include vesicle budding *into* the cytosol (normal topology membrane scission). Consistent with our hypothesis, previous examination of ESCRT-III activity on giant unilamellar vesicles (GUV) *in vitro* (Wollert et al., 2009) showed that while most vesicles formed intraluminally, vesicles could also bud *away from* the GUV. Also, cryo-EM images of purified ESCRT-III components demonstrated that ESCRT-III can deform and stabilize membranes for

normal-topology scission (McCullough et al., 2015). ESCRT-III has also been implicated in unconventional protein secretion from the ER with its mode of action unclear (Curwin et al., 2016). It is interesting to note that unconventional protein secretion has previously been linked to peroxisomes (Manjithaya et al., 2010), and may more broadly share a common mechanism of egress with PPVs from the ER. The expanding role of ESCRT-III in diverse cellular activities, including the formation of peroxisomes, suggests that this evolutionarily ancient protein complex has had a much greater influence on the sculpting of the eukaryotic bauplan than previously realized.

## Materials and Methods

### Yeast strains

The yeast strains used in this study are listed in Table S1 and were derived from the parental strain *BY4742* or the corresponding gene deletion strain library (Invitrogen) (Giaever et al., 2002), and as described previously (Mast et al., 2016).

### Yeast media and growth conditions

Yeast strains were grown in YPD (1% yeast extract, 2% peptone, 2% glucose) or YPBO (0.5% KPi, pH 6.0, 0.3% yeast extract, 0.5% peptone, 0.5 % Tween 40, 0.15% oleic acid), as indicated. All cultures were grown at 30°C. When marker selection was required for each strain, defined synthetic medium (SM) supplemented with 2% glucose and the necessary amino acid(s) or drug was used. Yeast media and growth conditions for specific experiments are listed below.

YPB-Oleate medium for use in ODELAY! was prepared as follows. A solution of 300 mg of methyl-β-cyclodextrin (Sigma)/mL and 10µL oleic acid/mL was prepared in absolute ethanol for a total volume of 3 mL. The solution was then placed in a Rotovap for 3 hrs to remove the

ethanol. The resulting powder was then reconstituted using ultra-pure $H_2O$ to a total volume 3 mL. Meanwhile 15 mL of 1.33% agarose, 2 mL of 10× YPB medium, and 1 mL of ultra-pure $H_2O$ were melted in boiling water for 18 min. Then 2 mL of the oleate-cyclodextrin solution were added to the melted medium and vortexed to mix. The YPB-Oleate medium was then cast into molds and allowed to cool as described (Herricks et al., 2017). YPB-glucose medium was prepared similarly except 2 mL of 20% glucose were added instead of the oleate-carbon source. To study peroxisome biogenesis, strains were grown overnight to saturation in YPD and diluted the next morning by dilution in fresh YPD to an $OD_{600}$ = 0.2. Cells were then grown to logarithmic phase ($OD_{600}$ = 0.7-1) before being diluted again in YPD, this time supplemented with 2 µM doxycycline, and incubated for 18 hrs. The logarithmic phase cells were harvested by centrifugation, washed five times in YPD to remove doxycycline, resuspended in fresh YPD medium without doxycycline, inoculated into YPD medium at an $OD_{600}$ = 0.2, and cultured for an additional 12 hrs.

**One cell doubling evaluation of living arrays of yeast (ODELAY!)**

Sensitive, high-density, and multiparametric analysis of cell growth was performed as described (Herricks et al., 2017). Briefly, yeast was cultured in YPD medium in 96 well plates at 30˚C overnight. Cultures were diluted to an $OD_{600}$ = 0.09 and allowed to grow for 6 hrs at 30˚C. The cultures were then washed in YPB medium without a carbon source and diluted to an $OD_{600}$ = 0.02 and spotted onto YBP-Oleate agarose medium. The resulting cultures were then observed using time-lapse microscopy for 48 hrs with 30 min intervals between images. All images were collected on Leica DMI6000 microscopes equipped with 10× 0.3 NA lenses using bright field

microscopy. MATLAB scripts using the Micro-Manager interface controlled the image collection process (Edelstein et al., 2014).

Population growth rates were scored against each other using the equation:

$$Z_{mean} = \frac{1}{n}\sum_{i}^{n}\frac{d_i - \mu_i}{\sigma_i}$$

Where $d_i$ is the $i$th decile of query population doubling time, $\mu_i$ is the mean of the $i$th decile of the parent strains doubling time, and $\sigma_i$ is the standard deviation of the $i$th decile of the parent strain's doubling time. The mean and standard deviation deciles ($\mu_i$ and $\sigma_i$) were calculated from 16 separate *wild-type* and 8 separate deletion strain populations containing at least 200 individuals per replicate. All calculations were performed using MATLAB scripts (Herricks et al., 2017).

**Electron microscopy and quantification**

Experiments were performed as described (Tam et al., 2003). Image analysis to measure cell and peroxisome profiles was performed in Image J (National Institutes of Health).

**Fluorescence microscopy and quantification**

Experiments were performed as described previously (Mast et al., 2016). Briefly, 25 fields of view yielding at least 250 cells per strain per time point for Gpd1-GFP labelled cells and at least 75 cells per strain per time point for Pex3-GFP and Snf7-mCherry cells were acquired in a randomized fashion with brightfield or calcofluor white staining used to establish focus for each strain and time point. Images were acquired with a 100× 1.4 NA objective (Olympus) on a DeltaVision Elite High Resolution Microscope (GE Healthcare Life Sciences). Images were

deconvolved with the manufacturer's supplied deconvolution software (softWoRx) and an experimentally determined point spread function. Images were further processed using Imaris software (Bitplane), and object-based colocalisation analysis was performed using the "Spots" function as described (Mast et al., 2016). Experiments were performed in triplicate.

***In vitro* vesicle budding assay**

Experiments were performed as described (Mast et al., 2016). To complement PPV budding defects, cytosols were mixed 1:1 before addition to the reaction. For experiments with apyrase, PYCs and cytosols were incubated separately with 1 U of apyrase (Sigma), resuspended in reaction buffer (25 mM HEPES-KOH, pH 7.2, 115 mM potassium acetate, 2.5 mM $MgCl_2$, 250 mM sorbitol) for 20 min prior to starting the reaction. For experiments in which exogenous ATP was added back, only apyrase-treated PYCs that had been washed in reaction buffer were used. Alphaview (ProteinSimple) was used to quantify the chemiluminescence signal with values normalized between the negative *pex19*Δ PYCs only control (set to 0), and the positive *wild-type* cytosol plus ATP control (set to 100). Experiments were performed in triplicate.

**Online supplemental material**

Fig. S1 contains supporting data that shows the population doubling time histograms of all yeast strains measured by ODELAY!. Fig. S2 contains supporting data to show additional electron micrographs of the ESCRT-III deletion mutants revealing peroxisome morphology defects. Fig. S3 contains supporting data to show the budding efficiencies of PPVs from reactions containing cytosols isolated from ESCRT deletion strains. Table S1. contains supplemental information on the genetic background of the yeast strains used in this study as well as their origin of derivation.

**Acknowledgments**

We thank Alexis Kaushansky, Sanjeev Kumar, Maxwell Neal, and the rest of the Aitchison laboratory for helpful discussion and feedback on the manuscript.

This work was supported by a Foundation Grant from the CIHR to R.A.R. and by grants P50 GM076547 and P41 GM109824 from the National Institutes of Health to J.D.A. F.D.M is a postdoctoral fellow of the Canadian Institutes of Health Research (CIHR). The support of Ian Black and Jennifer Tolmie and the Global Foundation for Peroxisomal Disorders is gratefully acknowledged.

The authors declare no competing financial interests.

Author Contributions: F.D.M., R.A.R, and J.D.A. designed the experiments, analyzed the results and wrote the manuscript. F.D.M. performed all the experiments. R.A.R performed the electron microscopy experiments. T.H. performed the ODELAY! experiments and analysis. K.M.S and L.R.M assisted with the experiments. R.A.S contributed to the experimental design and analysis. All authors read and commented on the manuscript.

**References**

Agrawal, G., S.N. Fassas, Z.J. Xia, and S. Subramani. 2016. Distinct requirements for intra-ER sorting and budding of peroxisomal membrane proteins from the ER. *The Journal of cell biology*. 212:335-348.

Agrawal, G., S. Joshi, and S. Subramani. 2011. Cell-free sorting of peroxisomal membrane proteins from the endoplasmic reticulum. *Proceedings of the National Academy of Sciences of the United States of America*. 108:9113-9118.

Agrawal, G., and S. Subramani. 2016. De novo peroxisome biogenesis: Evolving concepts and conundrums. *Biochimica et biophysica acta*. 1863:892-901.

Babst, M., D.J. Katzmann, E.J. Estepa-Sabal, T. Meerloo, and S.D. Emr. 2002a. Escrt-III: an endosome-associated heterooligomeric protein complex required for mvb sorting. *Dev Cell*. 3:271-282.

Babst, M., D.J. Katzmann, W.B. Snyder, B. Wendland, and S.D. Emr. 2002b. Endosome-associated complex, ESCRT-II, recruits transport machinery for protein sorting at the multivesicular body. *Dev Cell*. 3:283-289.

Babst, M., T.K. Sato, L.M. Banta, and S.D. Emr. 1997. Endosomal transport function in yeast requires a novel AAA-type ATPase, Vps4p. *The EMBO journal*. 16:1820-1831.

Carlton, J.G., and J. Martin-Serrano. 2007. Parallels between cytokinesis and retroviral budding: a role for the ESCRT machinery. *Science*. 316:1908-1912.

Curwin, A.J., N. Brouwers, Y.A.M. Alonso, D. Teis, G. Turacchio, S. Parashuraman, P. Ronchi, and V. Malhotra. 2016. ESCRT-III drives the final stages of CUPS maturation for unconventional protein secretion. *eLife*. 5.

David, C., J. Koch, S. Oeljeklaus, A. Laernsack, S. Melchior, S. Wiese, A. Schummer, R. Erdmann, B. Warscheid, and C. Brocard. 2013. A combined approach of quantitative interaction proteomics and live-cell imaging reveals a regulatory role for endoplasmic reticulum (ER) reticulon homology proteins in peroxisome biogenesis. *Molecular & cellular proteomics : MCP*. 12:2408-2425.

Distel, B., R. Erdmann, S.J. Gould, G. Blobel, D.I. Crane, J.M. Cregg, G. Dodt, Y. Fujiki, J.M. Goodman, W.W. Just, J.A. Kiel, W.H. Kunau, P.B. Lazarow, G.P. Mannaerts, H.W. Moser, T. Osumi, R.A. Rachubinski, A. Roscher, S. Subramani, H.F. Tabak, T. Tsukamoto, D. Valle, I. van der Klei, P.P. van Veldhoven, and M. Veenhuis. 1996. A unified nomenclature for peroxisome biogenesis factors. *J Cell Biol*. 135:1-3.

Edelstein, A.D., M.A. Tsuchida, N. Amodaj, H. Pinkard, R.D. Vale, and N. Stuurman. 2014. Advanced methods of microscope control using muManager software. *J Biol Methods*. 1.

Fakieh, M.H., P.J. Drake, J. Lacey, J.M. Munck, A.M. Motley, and E.H. Hettema. 2013. Intra-ER sorting of the peroxisomal membrane protein Pex3 relies on its luminal domain. *Biol Open*. 2:829-837.

Garrus, J.E., U.K. von Schwedler, O.W. Pornillos, S.G. Morham, K.H. Zavitz, H.E. Wang, D.A. Wettstein, K.M. Stray, M. Cote, R.L. Rich, D.G. Myszka, and W.I. Sundquist. 2001. Tsg101 and the vacuolar protein sorting pathway are essential for HIV-1 budding. *Cell*. 107:55-65.

Giaever, G., A.M. Chu, L. Ni, C. Connelly, L. Riles, S. Veronneau, S. Dow, A. Lucau-Danila, K. Anderson, B. Andre, A.P. Arkin, A. Astromoff, M. El-Bakkoury, R. Bangham, R. Benito, S. Brachat, S. Campanaro, M. Curtiss, K. Davis, A. Deutschbauer, K.D. Entian, P. Flaherty, F. Foury, D.J. Garfinkel, M. Gerstein, D. Gotte, U. Guldener, J.H. Hegemann, S. Hempel, Z. Herman, D.F. Jaramillo, D.E. Kelly, S.L. Kelly, P. Kotter, D. LaBonte, D.C. Lamb, N. Lan, H. Liang, H. Liao, L. Liu, C. Luo, M. Lussier, R. Mao, P. Menard, S.L. Ooi, J.L. Revuelta, C.J. Roberts, M. Rose, P. Ross-Macdonald, B. Scherens, G. Schimmack, B. Shafer, D.D. Shoemaker, S. Sookhai-Mahadeo, R.K. Storms, J.N. Strathern, G. Valle, M. Voet, G. Volckaert, C.Y. Wang, T.R. Ward, J. Wilhelmy, E.A. Winzeler, Y. Yang, G. Yen, E. Youngman, K. Yu, H. Bussey, J.D. Boeke, M. Snyder, P. Philippsen, R.W. Davis, and M. Johnston. 2002. Functional profiling of the Saccharomyces cerevisiae genome. *Nature*. 418:387-391.

Guizetti, J., L. Schermelleh, J. Mantler, S. Maar, I. Poser, H. Leonhardt, T. Muller-Reichert, and D.W. Gerlich. 2011. Cortical constriction during abscission involves helices of ESCRT-III-dependent filaments. *Science*. 331:1616-1620.

Halbach, A., C. Landgraf, S. Lorenzen, K. Rosenkranz, R. Volkmer-Engert, R. Erdmann, and H. Rottensteiner. 2006. Targeting of the tail-anchored peroxisomal membrane proteins PEX26 and PEX15 occurs through C-terminal PEX19-binding sites. *Journal of cell science*. 119:2508-2517.

Henne, W.M., N.J. Buchkovich, and S.D. Emr. 2011. The ESCRT pathway. *Dev Cell*. 21:77-91.

Herricks, T., D.J. Dilworth, F.D. Mast, S. Li, J.J. Smith, A.V. Ratushny, and J.D. Aitchison. 2017. One-Cell Doubling Evaluation by Living Arrays of Yeast, ODELAY! *G3 (Bethesda)*. 7:279-288.

Hettema, E.H., W. Girzalsky, M. van Den Berg, R. Erdmann, and B. Distel. 2000. Saccharomyces cerevisiae pex3p and pex19p are required for proper localization and stability of peroxisomal membrane proteins. *The EMBO journal*. 19:223-233.

Hoepfner, D., D. Schildknegt, I. Braakman, P. Philippsen, and H.F. Tabak. 2005. Contribution of the endoplasmic reticulum to peroxisome formation. *Cell*. 122:85-95.

Igual, J.C., E. Matallana, C. Gonzalez-Bosch, L. Franco, and J.E. Perez-Ortin. 1991. A new glucose-repressible gene identified from the analysis of chromatin structure in deletion mutants of yeast SUC2 locus. *Yeast*. 7:379-389.

Jan, C.H., C.C. Williams, and J.S. Weissman. 2014. Principles of ER cotranslational translocation revealed by proximity-specific ribosome profiling. *Science*. 346:1257521.

Jimenez, A.J., P. Maiuri, J. Lafaurie-Janvore, S. Divoux, M. Piel, and F. Perez. 2014. ESCRT machinery is required for plasma membrane repair. *Science*. 343:1247136.

Joshi, A.S., X. Huang, V. Choudhary, T.P. Levine, J. Hu, and W.A. Prinz. 2016. A family of membrane-shaping proteins at ER subdomains regulates pre-peroxisomal vesicle biogenesis. *The Journal of cell biology*. 215:515-529.

Katzmann, D.J., M. Babst, and S.D. Emr. 2001. Ubiquitin-dependent sorting into the multivesicular body pathway requires the function of a conserved endosomal protein sorting complex, ESCRT-I. *Cell*. 106:145-155.

Katzmann, D.J., C.J. Stefan, M. Babst, and S.D. Emr. 2003. Vps27 recruits ESCRT machinery to endosomes during MVB sorting. *The Journal of cell biology*. 162:413-423.

Lam, S.K., N. Yoda, and R. Schekman. 2010. A vesicle carrier that mediates peroxisome protein traffic from the endoplasmic reticulum. *Proceedings of the National Academy of Sciences of the United States of America*. 107:21523-21528.

Lee, J.A., A. Beigneux, S.T. Ahmad, S.G. Young, and F.B. Gao. 2007. ESCRT-III dysfunction causes autophagosome accumulation and neurodegeneration. *Current biology : CB*. 17:1561-1567.

Loncle, N., M. Agromayor, J. Martin-Serrano, and D.W. Williams. 2015. An ESCRT module is required for neuron pruning. *Sci Rep*. 5:8461.

Manjithaya, R., C. Anjard, W.F. Loomis, and S. Subramani. 2010. Unconventional secretion of Pichia pastoris Acb1 is dependent on GRASP protein, peroxisomal functions, and autophagosome formation. *The Journal of cell biology*. 188:537-546.

Mast, F.D., A. Jamakhandi, R.A. Saleem, D.J. Dilworth, R.S. Rogers, R.A. Rachubinski, and J.D. Aitchison. 2016. Peroxins Pex30 and Pex29 Dynamically Associate with Reticulons to Regulate Peroxisome Biogenesis from the Endoplasmic Reticulum. *The Journal of biological chemistry*. 291:15408-15427.

Mast, F.D., R.A. Rachubinski, and J.D. Aitchison. 2015. Signaling dynamics and peroxisomes. *Current opinion in cell biology*. 35:131-136.

McCullough, J., A.K. Clippinger, N. Talledge, M.L. Skowyra, M.G. Saunders, T.V. Naismith, L.A. Colf, P. Afonine, C. Arthur, W.I. Sundquist, P.I. Hanson, and A. Frost. 2015. Structure and membrane remodeling activity of ESCRT-III helical polymers. *Science*. 350:1548-1551.

Motley, A.M., P.C. Galvin, L. Ekal, J.M. Nuttall, and E.H. Hettema. 2015. Reevaluation of the role of Pex1 and dynamin-related proteins in peroxisome membrane biogenesis. *The Journal of cell biology*. 211:1041-1056.

Motley, A.M., and E.H. Hettema. 2007. Yeast peroxisomes multiply by growth and division. *The Journal of cell biology*. 178:399-410.

Olmos, Y., L. Hodgson, J. Mantell, P. Verkade, and J.G. Carlton. 2015. ESCRT-III controls nuclear envelope reformation. *Nature*. 522:236-239.

Perry, R.J., F.D. Mast, and R.A. Rachubinski. 2009. Endoplasmic reticulum-associated secretory proteins Sec20p, Sec39p, and Dsl1p are involved in peroxisome biogenesis. *Eukaryotic cell*. 8:830-843.

Rusten, T.E., T. Vaccari, K. Lindmo, L.M. Rodahl, I.P. Nezis, C. Sem-Jacobsen, F. Wendler, J.P. Vincent, A. Brech, D. Bilder, and H. Stenmark. 2007. ESCRTs and Fab1 regulate distinct steps of autophagy. *Current biology : CB*. 17:1817-1825.

Saleem, R.A., B. Knoblach, F.D. Mast, J.J. Smith, J. Boyle, C.M. Dobson, R. Long-O'Donnell, R.A. Rachubinski, and J.D. Aitchison. 2008. Genome-wide analysis of signaling networks regulating fatty acid-induced gene expression and organelle biogenesis. *The Journal of cell biology*. 181:281-292.

Saleem, R.A., R. Long-O'Donnell, D.J. Dilworth, A.M. Armstrong, A.P. Jamakhandi, Y. Wan, T.A. Knijnenburg, A. Niemisto, J. Boyle, R.A. Rachubinski, I. Shmulevich, and J.D. Aitchison. 2010. Genome-wide analysis of effectors of peroxisome biogenesis. *PloS one*. 5:e11953.

Scheffer, L.L., S.C. Sreetama, N. Sharma, S. Medikayala, K.J. Brown, A. Defour, and J.K. Jaiswal. 2014. Mechanism of Ca(2)(+)-triggered ESCRT assembly and regulation of cell membrane repair. *Nature communications*. 5:5646.

Schoneberg, J., I.H. Lee, J.H. Iwasa, and J.H. Hurley. 2016. Reverse-topology membrane scission by the ESCRT proteins. *Nature reviews. Molecular cell biology*.

Schrader, M., J.L. Costello, L.F. Godinho, A.S. Azadi, and M. Islinger. 2016. Proliferation and fission of peroxisomes - An update. *Biochimica et biophysica acta*. 1863:971-983.

Schuldiner, M., J. Metz, V. Schmid, V. Denic, M. Rakwalska, H.D. Schmitt, B. Schwappach, and J.S. Weissman. 2008. The GET complex mediates insertion of tail-anchored proteins into the ER membrane. *Cell*. 134:634-645.

Smith, J.J., and J.D. Aitchison. 2013. Peroxisomes take shape. *Nature reviews. Molecular cell biology*. 14:803-817.

Smith, J.J., Y. Sydorskyy, M. Marelli, D. Hwang, H. Bolouri, R.A. Rachubinski, and J.D. Aitchison. 2006. Expression and functional profiling reveal distinct gene classes involved in fatty acid metabolism. *Molecular systems biology*. 2:2006 0009.

South, S.T., K.A. Sacksteder, X. Li, Y. Liu, and S.J. Gould. 2000. Inhibitors of COPI and COPII do not block PEX3-mediated peroxisome synthesis. *The Journal of cell biology*. 149:1345-1360.

Tam, Y.Y., A. Fagarasanu, M. Fagarasanu, and R.A. Rachubinski. 2005. Pex3p initiates the formation of a preperoxisomal compartment from a subdomain of the endoplasmic reticulum in Saccharomyces cerevisiae. *The Journal of biological chemistry*. 280:34933-34939.

Tam, Y.Y., J.C. Torres-Guzman, F.J. Vizeacoumar, J.J. Smith, M. Marelli, J.D. Aitchison, and R.A. Rachubinski. 2003. Pex11-related proteins in peroxisome dynamics: a role for the novel peroxin Pex27p in controlling peroxisome size and number in Saccharomyces cerevisiae. *Molecular biology of the cell*. 14:4089-4102.

Tang, S., W.M. Henne, P.P. Borbat, N.J. Buchkovich, J.H. Freed, Y. Mao, J.C. Fromme, and S.D. Emr. 2015. Structural basis for activation, assembly and membrane binding of ESCRT-III Snf7 filaments. *eLife*. 4.

Thoms, S., I. Harms, K.U. Kalies, and J. Gartner. 2012. Peroxisome formation requires the endoplasmic reticulum channel protein Sec61. *Traffic*. 13:599-609.

Titorenko, V.I., H. Chan, and R.A. Rachubinski. 2000. Fusion of small peroxisomal vesicles in vitro reconstructs an early step in the in vivo multistep peroxisome assembly pathway of Yarrowia lipolytica. *The Journal of cell biology*. 148:29-44.

Titorenko, V.I., and R.A. Rachubinski. 2000. Peroxisomal membrane fusion requires two AAA family ATPases, Pex1p and Pex6p. *The Journal of cell biology*. 150:881-886.

van der Zand, A., I. Braakman, and H.F. Tabak. 2010. Peroxisomal membrane proteins insert into the endoplasmic reticulum. *Molecular biology of the cell*. 21:2057-2065.

van der Zand, A., J. Gent, I. Braakman, and H.F. Tabak. 2012. Biochemically distinct vesicles from the endoplasmic reticulum fuse to form peroxisomes. *Cell*. 149:397-409.

Vietri, M., K.O. Schink, C. Campsteijn, C.S. Wegner, S.W. Schultz, L. Christ, S.B. Thoresen, A. Brech, C. Raiborg, and H. Stenmark. 2015. Spastin and ESCRT-III coordinate mitotic spindle disassembly and nuclear envelope sealing. *Nature*. 522:231-235.

Webster, B.M., P. Colombi, J. Jager, and C.P. Lusk. 2014. Surveillance of nuclear pore complex assembly by ESCRT-III/Vps4. *Cell*. 159:388-401.

Wollert, T., C. Wunder, J. Lippincott-Schwartz, and J.H. Hurley. 2009. Membrane scission by the ESCRT-III complex. *Nature*. 458:172-177.

## Figure Legends

**Figure 1. ESCRT-III mutants have severe oleate-specific growth defects.** Doubling times of individual yeast cells growing into colonies on solid-phase medium containing either glucose or oleic acid as sole carbon source were measured with ODELAY!. A population-derived z-score and standard error-of-the-mean (SEM) for each strain are plotted with measurements from glucose-containing medium on the *x*-axis against measurements from oleic acid-containing medium on the *y*-axis from 8 biological replicates per growth condition. *vps20*Δ cells grew but

did not divide on medium containing oleic acid, so only the mean Z-score and SEM for growth on medium containing glucose are displayed.

**Figure 2. ESCRT-III deletion strains have reduced and aberrant peroxisome populations.** (A) *Wild-type*, (B) *vps20*Δ, and (C) *snf7*Δ cells were grown in medium containing oleic acid to induce peroxisomes and then prepared for electron microscopy. Cell ultrastructure and representative organelle profiles are depicted in a. Arrowheads in (B) and (C) point to aberrant peroxisomes. Bar = 1 µm. (D–I) Morphometric analysis of peroxisomes. For each strain analyzed, the areas of individual peroxisomes were determined. Bar graphs display the numerical density of peroxisomes (D) and the population distribution of the area of peroxisomes (E–I) for *wild-type* and ESCRT-III deletion strains.

**Figure 3. Vps20 and Snf7 positively regulate *de novo* peroxisome biogenesis.** (A) Genomically encoded *PEX19* was placed under the control of a tetracycline-repressible Tet07 promoter to allow regulatable *de novo* peroxisome production in *wild-type*, *vps20*Δ, and *snf7*Δ cells expressing Gpd1-GFP as a peroxisomal marker. Cells were imaged before (control) and after an 18 hr incubation with 2 µM doxycycline (+DOX), and 12 hrs after the removal of doxycyline (recovery). The percentage of cells containing peroxisomes and the average number of peroxisomes per cell in peroxisome-positive cells were measured at each time point and are depicted in bar plots with error bars representing the SEM of 3 biological replicates. Scale bar = 5 µm. (B) Snf7 localizes to sites of *de novo* peroxisome biogenesis. *Wild-type* cells expressing endogenously tagged Pex3-GFP and Snf7-mCherry with tetracycline-repressible *PEX19* were imaged before (control) and 1 hr following an 18 hr incubation with 2 µM doxycycline (recovery). Arrowheads point to areas of colocalization, see zoom window for enlargement. For

the merged image, calcofluor white staining (cyan) was used to demarcate cell boundaries. Bar graphs report the percent overlap of Pex3-GFP puncta colocalizing with Snf7-mCherry puncta with error bars representing the SEM of 3 biological replicates. Scale bar = 5 µm.

**Figure 4. Vps20 and Snf7 are required for budding of PPVs from the ER.** (A) Permeabilized *pex19*Δ yeast cells (PYCs) containing microsomes and expressing Pex3-GFP were incubated with the S100 fraction of cytosol isolated from *wild-type* (lanes 2 – 4), *vps25*Δ (lane 5), *vps20*Δ (lanes 6 and 8), *snf7*Δ (lanes 7 – 9) or *pex19*Δ (lanes 9 and 10) for 90 min at room temperature in the presence of an ATP-regenerating system. Controls included incubating the PYCs alone (lane 1), with cytosol but no ATP (lane 2) or with cytosol and ATP, but at 4 ˚C (lane 3). (B) ATP is not required for PPV release but rather to recycle scission components. PYCs and the S100 fraction of cytosol isolated from *wild-type* were pretreated with apyrase before starting the reaction (lanes 3 and 5). A time course was also performed at the indicated time points (lanes 6 – 10).

**Table 1. Average area and numerical density of peroxisomes in cells of *wild-type* and ESCRT-III deletion strains.**

| strain | cell area assayed (µm$^2$) | peroxisome count | numerical density of peroxisomes | average area of peroxisomes (µm$^2$) |
|---|---|---|---|---|
| *BY4742* | 1396.09 | 421 | 1.14 | 0.037 |
| *vps20*Δ* | 1125.46 | 69 | 0.39 | 0.005 |
| *snf7*Δ* | 1144.83 | 89 | 0.34 | 0.018 |
| *did4*Δ | 820.13 | 35 | 0.28 | 0.040 |
| *vps24*Δ | 933.70 | 138 | 0.51 | 0.044 |

* denotes peroxisome-like structures present.

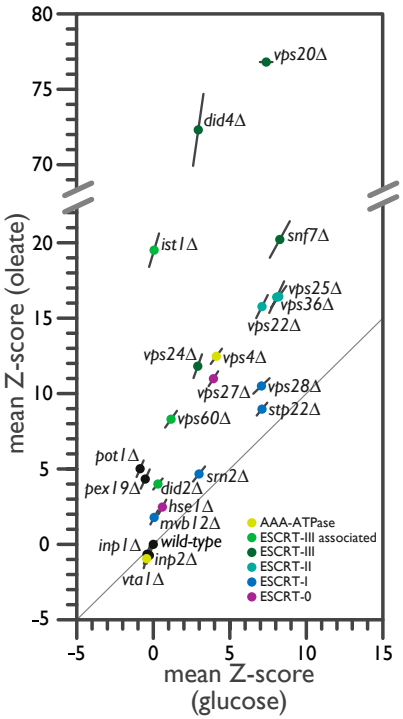

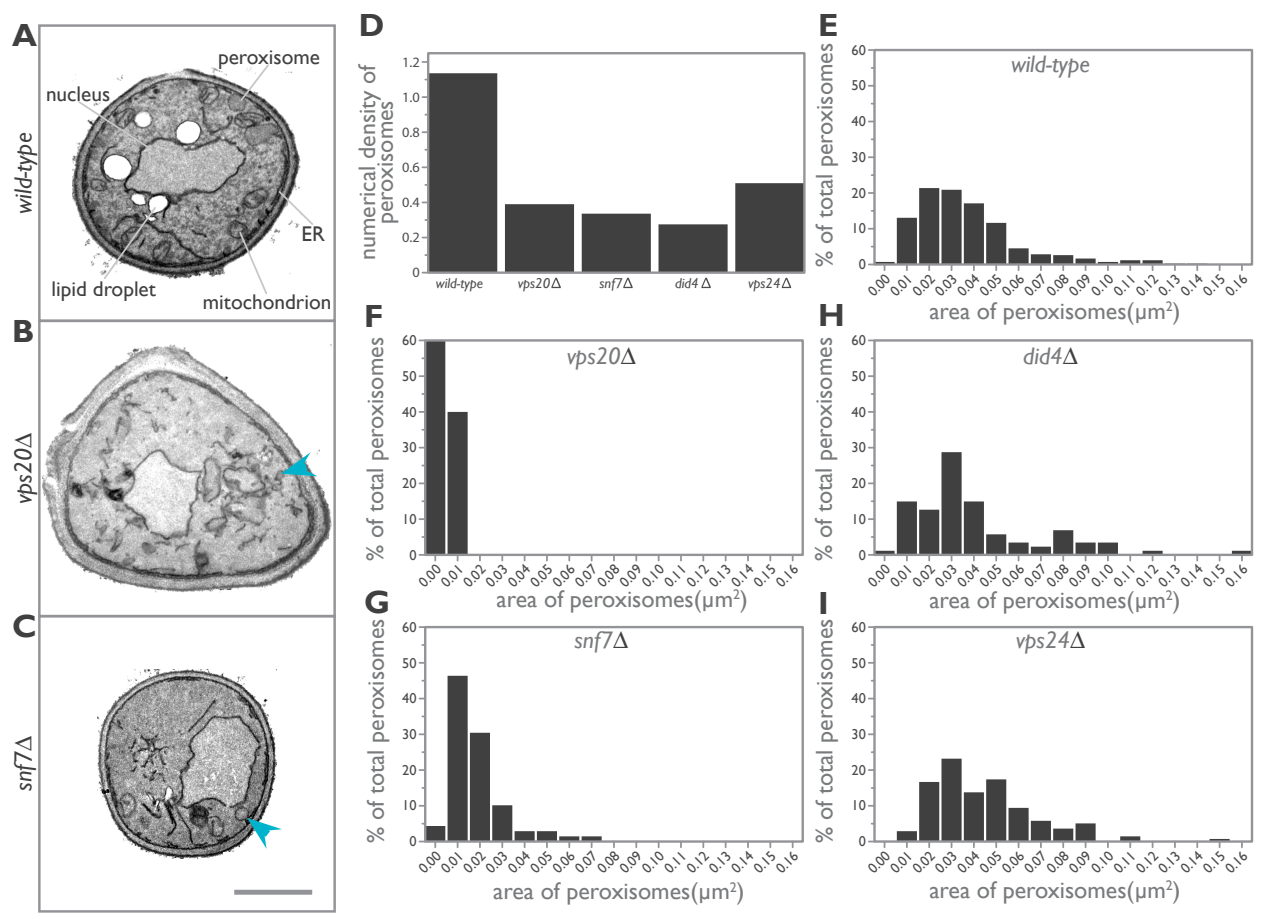
A
wild-type
peroxisome
nucleus
ER
lipid droplet
mitochondrion
B
vps20Δ
C
snf7Δ
D
numerical density of peroxisomes
wild-type
vps20Δ
snf7Δ
did4Δ
vps24Δ
E
wild-type
% of total peroxisomes
area of peroxisomes(μm²)
F
vps20Δ
G
snf7Δ
H
did4Δ
I
vps24Δ

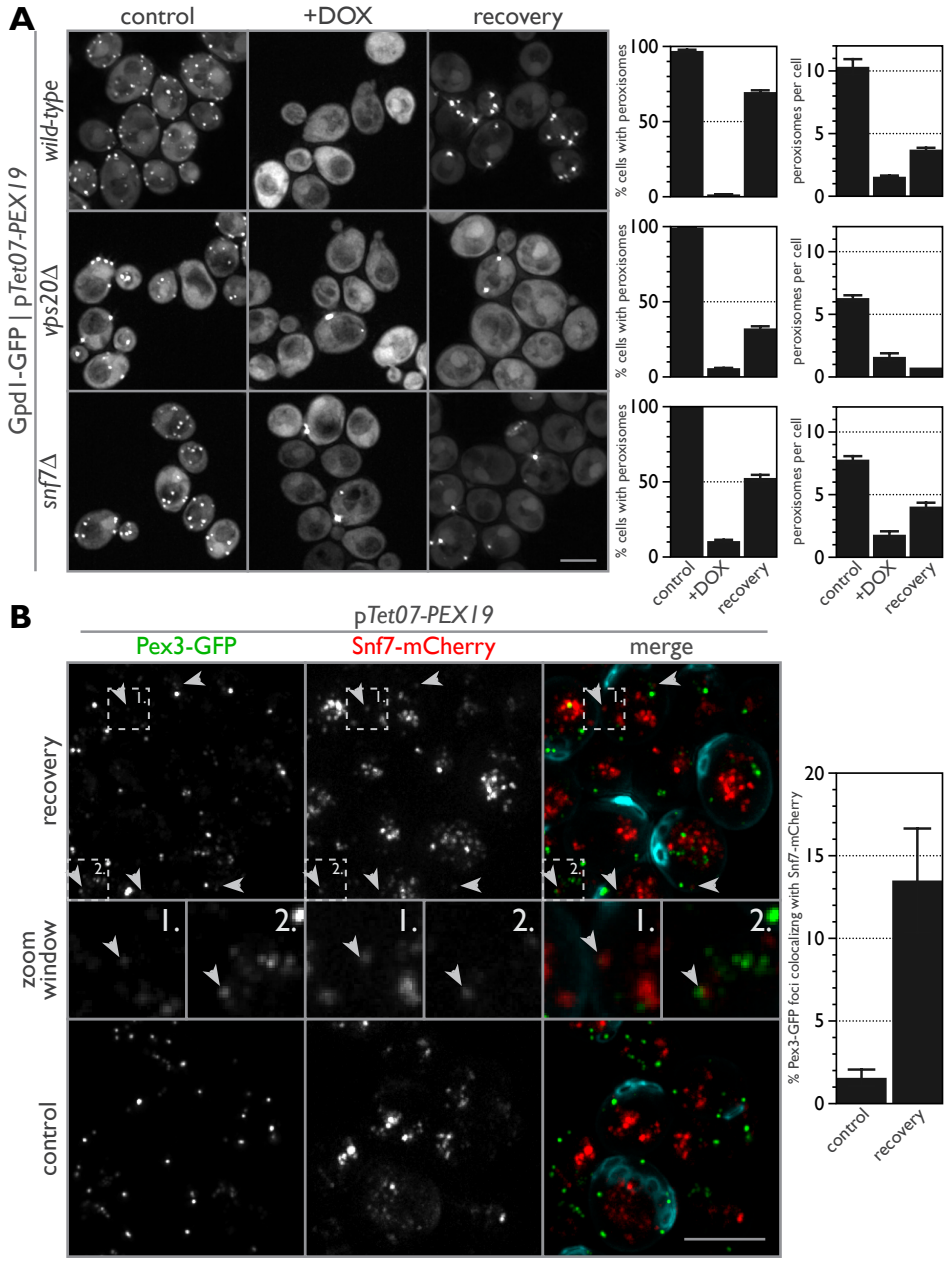

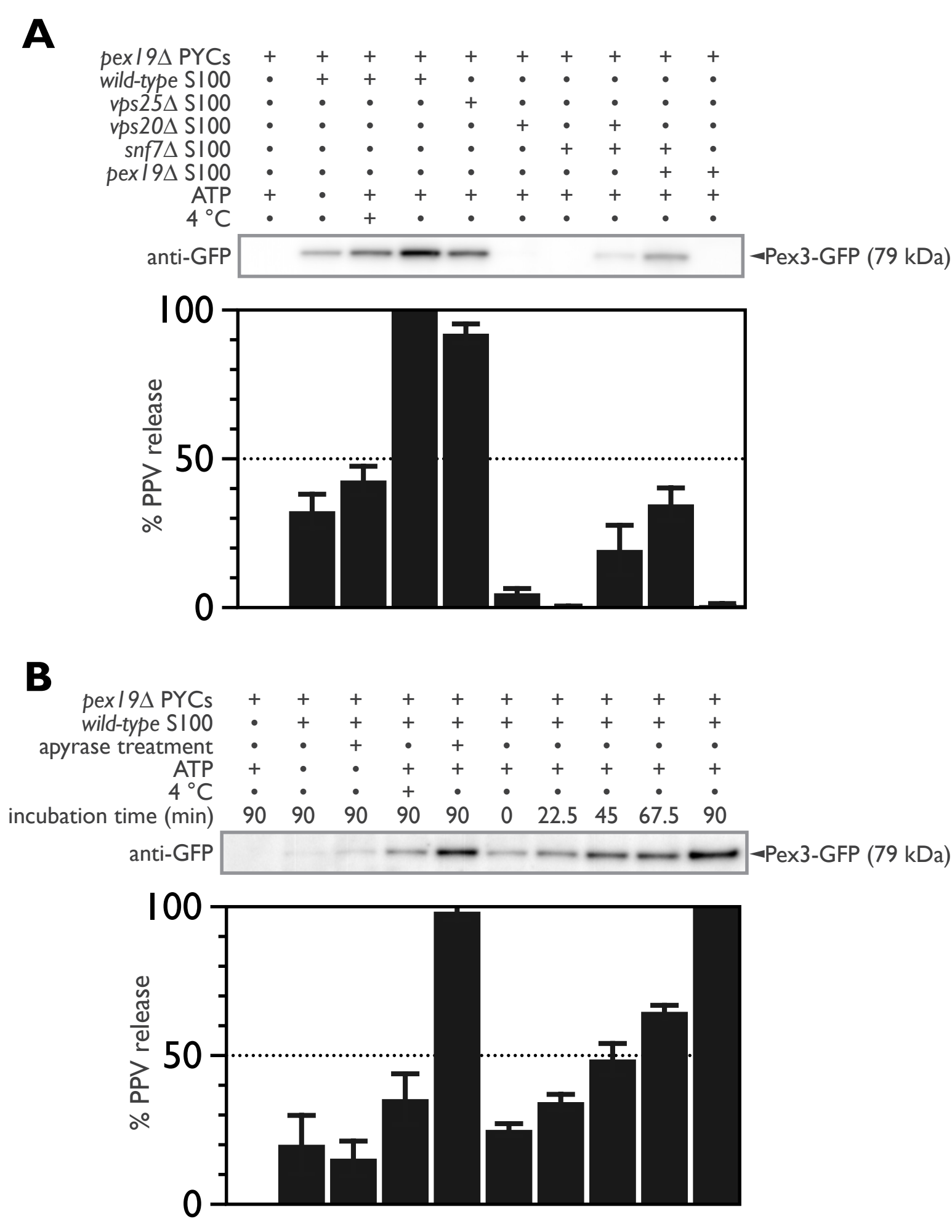
A
pex19Δ PYCs + + + + + + + + + +
wild-type S100 • + + + • • • • • •
vps25Δ S100 • • • • + • • • • •
vps20Δ S100 • • • • • + • + • •
snf7Δ S100 • • • • • • + + + •
pex19Δ S100 • • • • • • • • + +
ATP + • + + + + + + + +
4 °C • • + • • • • • • •
anti-GFP
Pex3-GFP (79 kDa)
100
50
0
% PPV release
B
pex19Δ PYCs + + + + + + + + + +
wild-type S100 • + + + + + + + + +
apyrase treatment • • + • + • • • • •
ATP + • • + + + + + + +
4 °C • • • + • • • • • •
incubation time (min) 90 90 90 90 90 0 22.5 45 67.5 90
anti-GFP
Pex3-GFP (79 kDa)
100
50
0
% PPV release